Ezrin regulates focal adhesion and invadopodia dynamics by altering calpain activity to promote breast cancer cell invasion

Victoria Hoskin[a,b], Alvin Szeto[a,b], Abdi Ghaffari[a,b], Peter A. Greer[a,b], Graham P. Côté[c], and Bruce E. Elliott[a,b]

[a]Division of Cancer Biology and Genetics, Cancer Research Institute, [b]Department of Pathology and Molecular Medicine, and [c]Department of Biomedical and Molecular Sciences, Queen's University, Kingston, ON K7L 3N6, Canada

ABSTRACT **Up-regulation of the cytoskeleton linker protein ezrin frequently occurs in aggressive cancer types and is closely linked with metastatic progression. However, the underlying molecular mechanisms detailing how ezrin is involved in the invasive and metastatic phenotype remain unclear. Here we report a novel function of ezrin in regulating focal adhesion (FA) and invadopodia dynamics, two key processes required for efficient invasion to occur. We show that depletion of ezrin expression in invasive breast cancer cells impairs both FA and invadopodia turnover. We also demonstrate that ezrin-depleted cells display reduced calpain-mediated cleavage of the FA and invadopodia-associated proteins talin, focal adhesion kinase (FAK), and cortactin and reduced calpain-1–specific membrane localization, suggesting a requirement for ezrin in maintaining proper localization and activity of calpain-1. Furthermore, we show that ezrin is required for cell directionality, early lung seeding, and distant organ colonization but not primary tumor growth. Collectively our results unveil a novel mechanism by which ezrin regulates breast cancer cell invasion and metastasis.**

Monitoring Editor
Alpha Yap
University of Queensland

Received: Dec 11, 2014
Revised: Jul 21, 2015
Accepted: Jul 31, 2015

INTRODUCTION

The ability of cancer cells to migrate and invade beyond the boundaries of the primary tumor and into the surrounding stromal microenvironment represents a critical step in the dissemination process. Two prominent structures involved in cancer cell migration and invasion are integrin-based focal adhesions (FAs) and invadopodia, respectively. FAs are the main sites of cell–extracellular matrix (ECM) attachment that mediate activation of downstream signaling pathways important for cytoskeletal reorganization and the generation of traction forces during cell migration (Carragher and Frame, 2004). In contrast, invadopodia are specialized F-actin–rich membrane protrusions that secrete matrix-degrading proteases (e.g., matrix metalloproteinases [MMPs]; Linder, 2007). Both FAs and invadopodia are highly dynamic, transient structures requiring effective assembly and disassembly in order to facilitate migration and invasion (Franco *et al.*, 2004; Chan *et al.*, 2009) and are implicated in cancer metastasis (Deakin and Turner, 2011; Yamaguchi, 2012).

Structurally, FAs and invadopodia are quite distinct, yet they share many of the same constituent adhesion molecules, as well as mechanisms regulating their dynamics (Kaverina *et al.*, 1999; Kopp *et al.*, 2006; Zaidel-Bar *et al.*, 2007; Badowski *et al.*, 2008; Chan *et al.*, 2009), suggesting important interplay between these two multiprotein complexes. In particular, the cysteine protease calpain has been studied extensively in this context. Indeed, calpain is a critical promoter of both FA and invadopodia turnover through cleavage of specific substrates, by which inhibition of calpain or disrupting calpain-mediated cleavage of its substrates impairs FA and invadopodia turnover (Franco *et al.*, 2004; Calle *et al.*, 2006; Cortesio *et al.*, 2008; Chan *et al.*, 2010).

The membrane-cytoskeleton linker protein ezrin (EZR) is the only ezrin-radixin-moesin (ERM) family member known to be cleaved by calpain (Yao *et al.*, 1993), although little is known about the

This article was published online ahead of print in MBoC in Press (http://www.molbiolcell.org/cgi/doi/10.1091/mbc.E14-12-1584) on August 5, 2015.

Address correspondence to: Bruce E. Elliott (elliottb@queensu.ca).

Abbreviations used: ANOVA, analysis of variance; CAPN1, calpain-1 catalytic subunit; CAPN2, calpain-2 catalytic subunit; CAPNS1, calpain small subunit; ECM, extracellular matrix; ERM, ezrin-radixin-moesin; EV, empty vector; EZR, ezrin; FA, focal adhesion; FAK, focal adhesion kinase; GFP, green fluorescent protein; MMP, matrix metalloproteinase; PBS, phosphate-buffered saline; RFP, red fluorescent protein; WT, wild type.

significance of their interaction. Ezrin participates in several actin-based functions, including maintenance of epithelial cell polarity (Bretscher *et al.*, 2002) and microvilli organization (Saotome *et al.*, 2004), and a growing body of evidence implicates ezrin as an important regulator and promoter of tumor progression and metastasis (Khanna *et al.*, 2004; Yu *et al.*, 2004; Elliott *et al.*, 2005). Data from our lab and others have shown that overexpression of ezrin leads to increased cell scattering and invasion of cancer cells (Elliott *et al.*, 2004; Naba *et al.*, 2008), whereas disruption of ezrin function using mutational or RNA interference approaches abrogates metastatic spread (Khanna *et al.*, 2004; Mak *et al.*, 2012). Clinically, increased expression of ezrin is frequently found in invasive cancers, including breast cancer, where it is correlated with increased malignancy and poor overall survival (Kobel *et al.*, 2006; Sarrio *et al.*, 2006; Bruce *et al.*, 2007; Elzagheid *et al.*, 2008). Data also suggest that high ezrin levels can predict the development of metastasis and local recurrence in soft tissue sarcomas (Carneiro *et al.*, 2011), emphasizing the clinical importance of up-regulated ezrin expression and the need to better understand its role as a metastasis-associated protein.

Although a requirement for ezrin in cancer cell invasion and metastasis has been demonstrated, what remain unclear are the underlying molecular mechanisms by which ezrin drives the invasive phenotype. In this study, we investigate the function of ezrin in regulating FA and invadopodia dynamics. Our findings highlight novel functions of ezrin in regulating cancer cell invasion and metastasis by promoting FA and invadopodia turnover through regulation of calpain-1 activity, as well as colonization at distant organ sites.

RESULTS

Ezrin regulates focal adhesion turnover and cell adhesion

Previous studies demonstrated a critical role for ezrin in maintaining epithelial integrity as well as for cell spreading and migration in cancer cells (Bretscher *et al.*, 2002; Srivastava *et al.*, 2005; Prag *et al.*, 2007). However, the role of ezrin in FA dynamics and ECM attachment, which are tightly regulated in migrating cells, has not been characterized. To this end, we generated ezrin-deficient MDA-MB-231 (MDA231) breast cancer cells using two independent short hairpin RNA (shRNA) constructs that depleted endogenous ezrin by at least 75% (Supplemental Figure S1A). Surprisingly, the number and size of FAs, as judged by staining for three different FA proteins—paxillin, vinculin, and FA kinase (FAK)—were significantly increased in ezrin-depleted cells compared with control (empty vector [EV] transduced, MDA231-EV; Figure 1, A–C, and Supplemental Figure S1, B–D). Furthermore, the number and size of FAs per cell remained consistent among all proteins assessed within the same cell line (Figure 1, B and C, and Supplemental Figure S1, C and D), thus providing validation of our FA readout. We also detected an increase in FAs containing zyxin (Figure 1D and Supplemental Figure S1E), which is a marker of stable, mature adhesions (Zaidel-Bar *et al.*, 2003, 2004). To determine whether ezrin regulates FA turnover, we used time-lapse fluorescence microscopy to visualize the dynamics of red fluorescent protein (RFP)–zyxin in control and ezrin-deficient MDA231 cells (Figure 2A). Ezrin-deficient cells showed ~50% reduction in disassembly rate with no significant change in the rate of assembly of FAs (Figure 2, B and C). Furthermore, the duration of FAs was significantly increased in ezrin-deficient cells (mean, >75 min) compared with control cells (mean, ~40 min; Figure 2D and Supplemental Videos S1 and S2), and resulted in an increase in the percentage of longer-lived versus short-lived FAs found at any given time within ezrin-depleted cells (Figure 2E).

Because ezrin depletion altered FA disassembly rates, we predicted that changes in cellular adhesion and potentially integrin engagement would ensue. Indeed, we observed increases in total FAK levels, as well as phosphorylation of Y397FAK (Supplemental Figure S2A), which is known to occur upon integrin engagement and clustering. In agreement with these results, we detected increased cell attachment to collagen-I and fibronectin ECM substrata (Supplemental Figure S2B), as well as increased β1 integrin total protein (Supplemental Figure S2C). No significant change in the expression of paxillin or vinculin was detected, although FAK and zyxin protein levels were elevated by ~35% and 20%, respectively (Supplemental Figure S2C). Collectively these findings indicate that ezrin promotes the disassembly and turnover of FAs in breast cancer cells.

Ezrin regulates Src-induced invadopodia dynamics but does not alter MMP activity

To determine whether ezrin affects invadopodia turnover, we used time-lapse fluorescence microscopy to visualize the invadopodia marker green fluorescent protein (GFP)–cortactin in MDA231 cells expressing constitutively active Src Y527F plus empty vector (MDASrc-EV cells) and in ezrin-deficient MDASrc cells (Figure 3A). We chose this approach because MDA231 cells readily form FAs, whereas exogenous expression of constitutively active Src strongly induces the formation of numerous cortactin-rich invadopodia compared with parental cells (Gavazzi *et al.*, 1989; Hu *et al.*, 2011). Similar to our FA dynamic studies, we observed that the rate of invadopodia disassembly was diminished by approximately fourfold in ezrin-deficient compared with control MDASrc-EV cells, whereas the assembly rate did not change (Figure 3, B and C). We also observed significantly more invadopodia spots in ezrin-deficient MDASrc cells, which had longer durations (mean, >30 min; Figure 3, D and E, and Supplemental Videos S3 and S4) and consequently a greater percentage of longer-lived versus shorter-lived invadopodia than with control MDASrc cells (Figure 3F).

To assess whether there was any change in proteolytic activity in ezrin-depleted MDASrc cells, we performed gelatin zymography and ECM-degradation assays. We did not detect any significant change in MMP-2 or MMP-9 activity between MDASrc-EV and ezrin-depleted cells (Figure 4A). However, we observed that ezrin depletion resulted in markedly larger nonfluorescent areas representing ECM degradation when cells were seeded onto a fluorescently labeled fibronectin-gelatin substratum (Figure 4B), which is likely attributable to the defect in disassembly kinetics and prolonged duration of invadopodia structures. Despite the increased number of invadopodia in ezrin-depleted MDASrc cells, both invasion through Matrigel and transendothelial migration were markedly impaired in these cells (Figure 4, C and D). Taken together, our results suggest a novel role for ezrin in invasion by promoting invadopodia turnover.

Ezrin regulates directional persistence and front–rear cell polarization

Because depletion of ezrin hinders FA and invadopodia turnover, we predicted that it would also perturb directional cell migration, as previous studies linked tail retraction—known to involve dynamic adhesions—and front–rear cell polarization to cell directionality (Theisen *et al.*, 2012; Chaki *et al.*, 2013). We therefore performed time-lapse differential interference contrast (DIC) microscopy to monitor the movement of MDA231-EV and ezrin-depleted cells. Using the open source computer program DiPer (Gorelik and Gautreau, 2014), we quantitatively assessed cell migration differences between control and ezrin-deficient cells using two different parameters: mean square displacement (MSD) and direction autocorrelation. MSD is a measure of the surface area explored by cells over time and therefore provides information regarding the overall

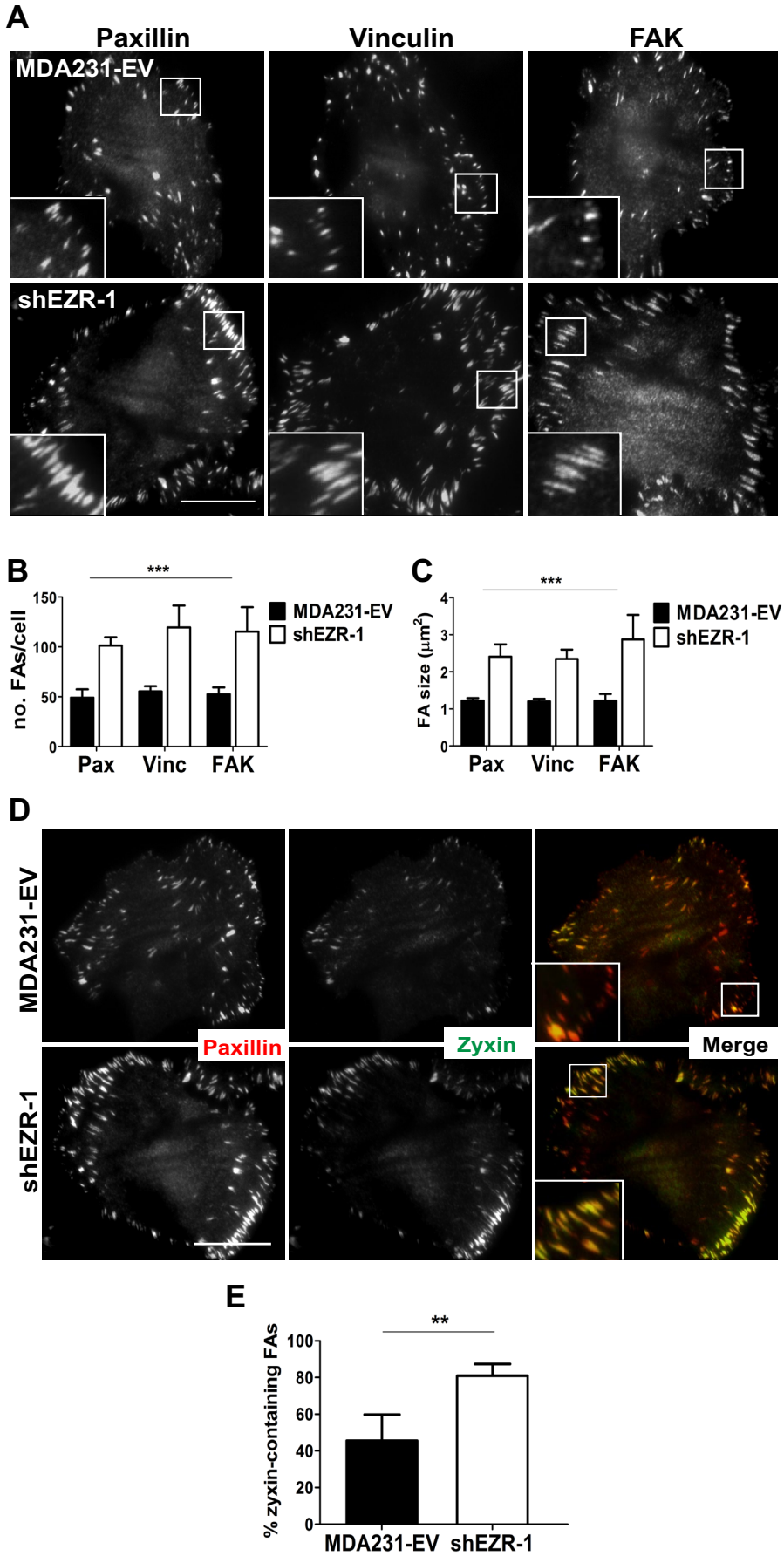

efficiency of cell migration. Direction autocorrelation is used as a measure of directional persistence, as it describes how the angle of displacement vectors tangential to a cell's trajectory align with each other over different time points, and is reflective of a cell's propensity to turn/change direction (Gorelik and Gautreau, 2014). Cell trajectories from ezrin-deficient cells were shorter and more convoluted than with control cells, which exhibited relatively straighter paths (Figure 5A). MSD values for ezrin-deficient cells were substantially lower across all time points analyzed, and their direction autocorrelation curves decayed significantly faster than those of control cells (Figure 5, B and C). Similar results were obtained with MDASrc-EV and MDASrc ezrin-depleted cells (Supplemental Figure S3). Collectively these data suggest that ezrin- deficient cells exhibit reduced migration efficiency, are more likely to turn, and therefore show reduced directional persistence.

We next examined the morphology of MDA231-EV and ezrin-depleted cells to determine whether ezrin depletion affects the front–rear axis of polarization. MDA231-EV cells exhibited organized stress fibers aligned in a front–rear manner, consistent with a polarized morphology, whereas ezrin-deficient cells were significantly less polarized and much flatter and displayed stress fibers with little or no front–rear organization (Figure 5D). We quantified these changes in cellular morphology using cell area as a measure of flatness (Figure 5E) and the presence or absence of aligned stress fibers to distinguish polarized versus nonpolarized cells (Figure 5F). As

FIGURE 1: Ezrin regulates FA stability. (A) MDA231-EV and ezrin-depleted cells stained by immunofluorescence with anti-paxillin, anti-vinculin, or anti-FAK antibodies and imaged using TIRF microscopy. Boxed areas depict regions of FAs that are magnified in insets (100×). (B, C) Quantification of the number and size of FAs. (D) Cells stained by immunofluorescence using anti-paxillin and anti-zyxin antibodies and imaged using TIRF microscopy. (E) The percentage of zyxin-containing FAs was quantified by dividing the number of FAs in which zyxin and paxillin colocalized by the total number of paxillin-containing FAs counted. Data shown represent means + SD of at least three independent experiments. A minimum of 30 cells per FA protein were analyzed. $^{**}p < 0.01$ by unpaired *t* test (E); $^{***}p < 0.0001$ by two-way ANOVA comparing all shEZR-1 to MDA231-EV values (B, C). Scale bars, 15 μm.

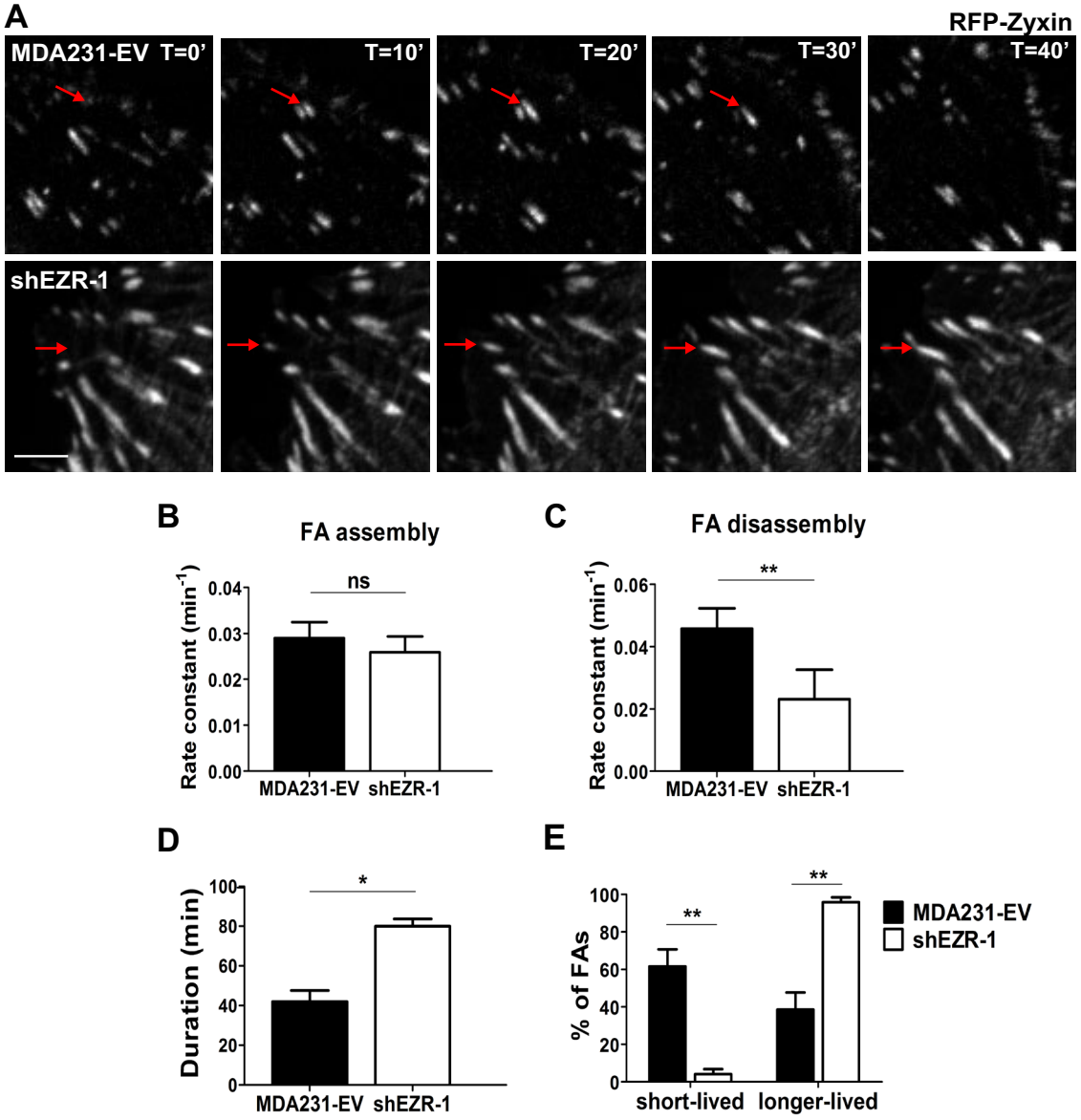

FIGURE 2: Ezrin is required for proper FA turnover. (A) RFP-zyxin was transiently transfected into MDA231-EV and ezrin-depleted (shEZR-1) cells and analyzed by time-lapse fluorescence microscopy for a minimum of 3 h. Images are representative of the dynamics of the FA marker RFP-zyxin over a period of 40 min. Red arrows indicate FAs. Scale bar, 5 μm. Rate constants for assembly (B) and disassembly (C) were calculated as described in *Materials and Methods*. (D) The mean duration of FAs for each cell type was calculated. (E) The percentage of short- and longer-lived FAs was quantified, with short-lived adhesions defined as those that formed and disassembled within 40 min; any FAs with a duration >40 min were counted as longer lived. Data shown represent means + SD of three independent experiments, with a minimum of 40 FAs analyzed per experiment. *$p < 0.02$ and ** $p < 0.007$ by unpaired *t* test (C, D) or two-way ANOVA (E); ns, not significant.

an independent assessment of front–rear polarization, the axial ratio (length/width) of cells was calculated (Grande-Garcia *et al.*, 2007). MDA231-EV cells consistently had an elliptical factor of at least 1.5 (indicative of an elongated and polarized morphology), whereas ezrin-depleted cells had a mean elliptical factor of 1 (Figure 5G), suggesting a loss of front–rear polarized morphology.

Ezrin regulates activity and localization of calpain

Multiple lines of evidence suggest that FA and invadopodia turnover are regulated by similar pathways. Indeed, calpain has been causally linked to promoting FA and invadopodia/podosome disassembly through cleavage of its substrates, including talin (Franco *et al.*, 2004), FAK (Chan *et al.*, 2010), and cortactin (Cortesio *et al.*, 2008). Ezrin is also a substrate specifically of calpain-1 (Yao *et al.*, 1993; Shuster and Herman, 1995; Dewitt and Hallett, 2007), whereas other ERMs, such as moesin, are insensitive to proteolytic cleavage by calpain (Shcherbina *et al.*, 1999). However, it is not known whether ezrin is involved in regulating calpain-mediated FA and invadopodia turnover. To this end, we assessed relative changes in the levels of talin and FAK cleavage by immunoblot analysis in MDA231-EV cells and cortactin cleavage in MDASrc-EV cells as indicators of calpain-mediated FA and invadopodia turnover, respectively. To validate the specificity of the calpain cleavage products, we depleted the catalytic subunits of

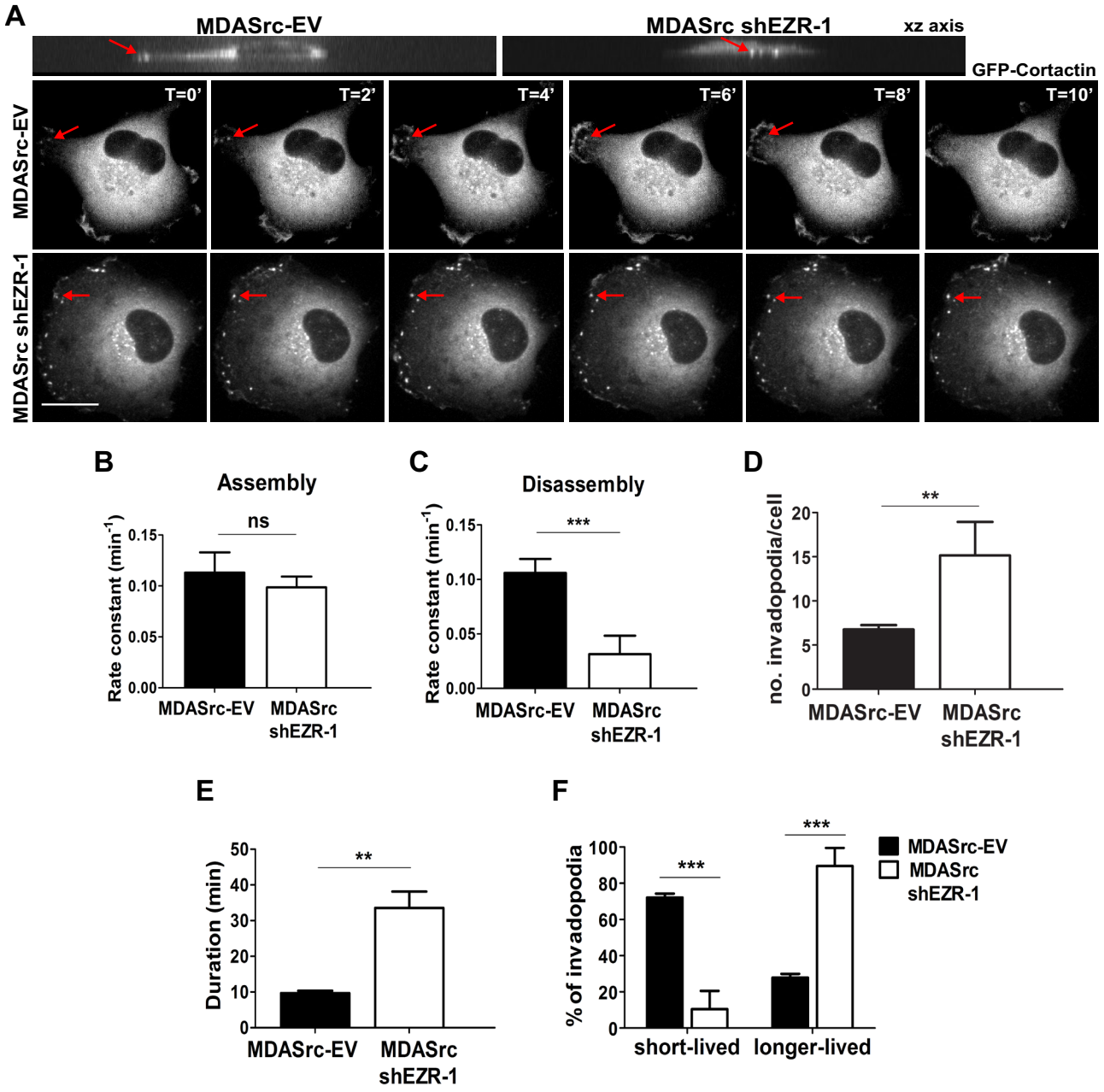

FIGURE 3: Ezrin regulates Src-induced invadopodia dynamics. (A) GFP-cortactin was transiently transfected into MDASrc-EV and MDASrc ezrin-depleted (MDASrc shEZR-1) cells and analyzed by time-lapse fluorescence microscopy for a minimum of 3 h. Images are representative of the dynamics of GFP-cortactin over a period of 10 min. The *xy* images (top) demonstrate that the invadopodia that formed protrude downward into the matrix. Rate constants for the assembly (B) and disassembly (C) of invadopodia were calculated as described in *Materials and Methods*. Mean duration of invadopodia (D) and number of invadopodia per cell (E). (F) Percentage of short- and longer-lived invadopodia; invadopodia that formed and disassembled within 10 min were counted as short lived, and those that persisted for >10 min were considered longer lived. Data shown represent means + SD of three independent experiments. A minimum of 40 invadopodia was analyzed per experiment. $^{**}p < 0.01$ and $^{***}p < 0.001$ by unpaired *t* test (C–E) or two-way ANOVA (F); ns, not significant. Scale bar, 15 μm.

calpain-1 (CAPN1) and of calpain-2 (CAPN2) in MDA231 cells by targeting the obligate small regulatory subunit (CAPNS1) using lentiviral shRNA (Supplemental Figure S4). We observed significant reductions in calpain-mediated cleavage of all the foregoing molecules in ezrin-depleted MDA231 and MDASrc cells (Figure 6, A–C), suggesting that ezrin may regulate FA and invadopodia dynamics through calpain. Because cleavage of talin by calpain is also important for mediating turnover in invadopodia (Calle *et al.*, 2006), we assessed talin cleavage in MDASrc-EV and ezrin-depleted MDASrc cells. As expected, the calpain-generated cleavage product of talin was markedly reduced in MDASrc cells depleted of ezrin (Figure 6D). Together these results indicate that ezrin depletion reduces cleavage of specific calpain substrates involved in FA and invadopodia disassembly.

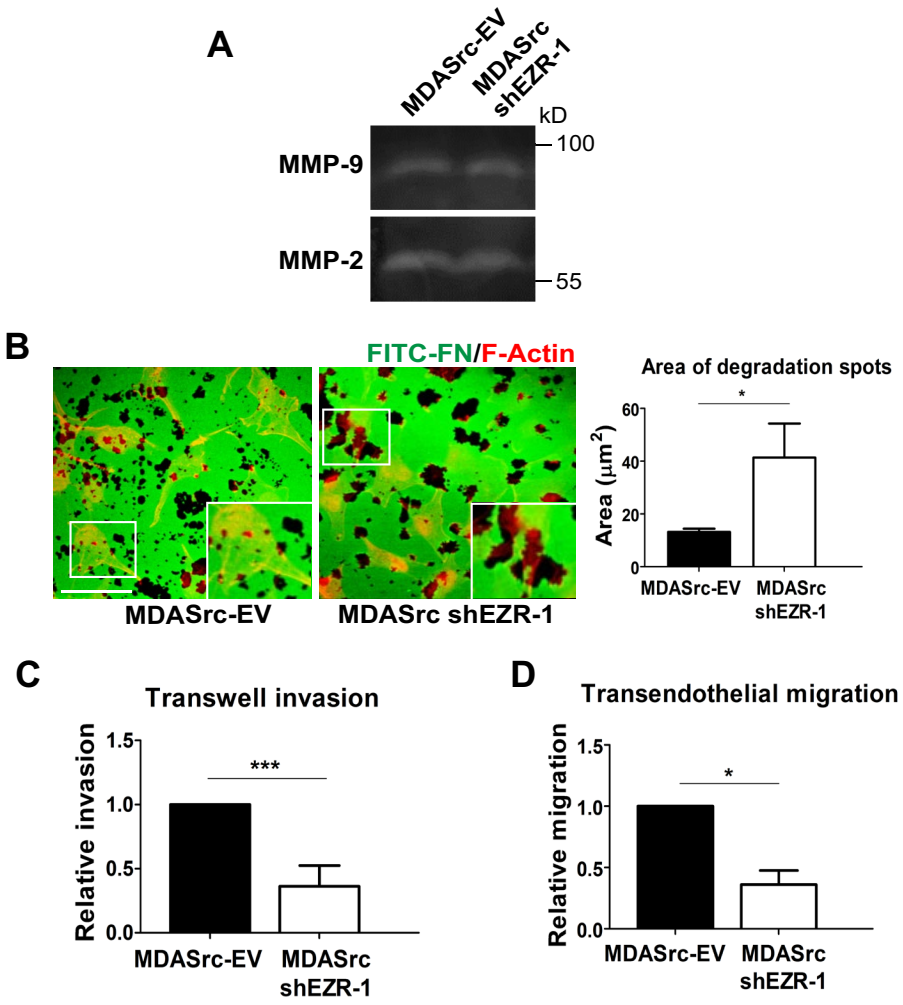

FIGURE 4: Ezrin does not regulate MMP secretion but is required for invasion and transendothelial migration. (A) Conditioned media from MDASrc-EV and ezrin-depleted MDASrc cells were collected and analyzed by gelatin zymography for MMP-2 and MMP-9 activity. (B) Cells were plated onto FITC-fibronectin gelatin coverslips for 72 h, fixed, and stained with F-actin (red). For each cell type, the total area of matrix digestion (dark spots) was calculated using ImagePro Plus 6.0 software. (C) Cells (5×10^4) were seeded onto Transwell inserts coated with 100 µl of 20% Matrigel and allowed to invade for 18 h. Invaded cells were stained with DAPI and quantified using Image ProPlus 6.0 software. (D) Cells (2×10^4) labeled with a green cell tracker were seeded onto an endothelial monolayer in a Transwell insert and allowed to migrate for 6 h. Invaded and migrated cells were quantified using Image ProPlus. Data shown represent means + SD of three independent experiments. *$p < 0.05$ and ***$p < 0.0001$ by unpaired *t* test (B) or one-sample *t* test (C, D). Scale bar, 30 µm.

We next examined the interaction between ezrin and calpain. Coimmunoprecipitation studies demonstrated that ezrin interacts with CAPN1 but not CAPN2 (Supplemental Figure S5A), consistent with previous reports indicating an ezrin–calpain-1 specific interaction (Yao *et al.*, 1993). Furthermore, double immunofluorescence staining for CAPN1 and ezrin show significant colocalization of these proteins at the cell membrane (Supplemental Figure S5B). Because localization of calpain to the cell periphery is important for its activity (Shao *et al.*, 2006; Leloup *et al.*, 2010) and active ezrin is found at the plasma membrane, we postulated that ezrin depletion might affect calpain-1 membrane localization. Immunofluorescence staining showed reduced CAPN1 at the plasma membrane in ezrin-depleted cells compared with control MDA231-EV cells (Figure 7A), whereas no change in CAPN2 membrane localization was detected (Supplemental Figure S5C). To confirm these observations, we performed cell fractionation experiments to isolate membrane and cytoplasmic fractions. We observed reduced amounts of CAPN1 but not CAPN2 at the membrane in ezrin-deficient cells (Figure 7B). Of interest, the cytoplasmic levels of CAPN1 were also reduced in ezrin-deficient cells, whereas cytoplasmic CAPN2 levels were unchanged (Figure 7B). We therefore looked at total protein levels in whole-cell lysates and found that CAPN1 but not CAPN2 was reduced by 50% in ezrin-deficient cells (Figure 7C), suggesting that ezrin may be regulating CAPN1 protein expression. We also looked at CAPN1 and CAPN2 mRNA expression and detected no change in the mRNA levels of either *capn1* or *capn2* (Figure 7D), indicating that the observed effects of ezrin depletion on CAPN1 protein expression are at the posttranscriptional level.

On the basis of these results, we next tested whether disrupting ezrin function at the plasma membrane would alter calpain-1 membrane localization. We first monitored talin cleavage in MDA231-EV and MDASrc-EV cells transiently overexpressing vector control (pCB6), wild-type (WT) ezrin, or a point mutant of ezrin (threonine-to-alanine 567 substitution [T/A]). The T/A ezrin mutant is not phosphorylatable at residue 567 and therefore not fully open or active but is still able to localize to the membrane (Gautreau *et al.*, 2000). Of interest, we observed a strong induction of calpain-mediated talin cleavage with WT ezrin compared with pCB6 control. However, the T/A ezrin mutant did not induce talin cleavage in MDA231-EV or MDASrc-EV cells but exhibited talin cleavage levels comparable to those of the pCB6 control (Figure 7E and Supplemental Figure S6). To test whether ezrin is important for the recruitment of calpain-1 to the plasma membrane, we isolated membrane and cytoplasmic fractions from pCB6 control, WT ezrin, and T/A ezrin–overexpressing MDA231-EV cells. Our results showed that WT ezrin induced CAPN1 membrane localization, whereas T/A ezrin did not (Figure 7F). CAPN2 membrane localization on the other hand remained unchanged between WT and T/A ezrin–overexpressing cells (Figure 7F and Supplemental Figure 5D), similar to the cytoplasmic and total levels of CAPN1 and CAPN2 levels. Taken together, these results suggest that the open and active ezrin conformation is important for promoting membrane localization specifically for calpain-1 and regulating calpain proteolytic activity toward talin.

Ezrin is required for initial lung seeding and colonization events in vivo

Our lab (Elliott *et al.*, 2005) and others (Khanna *et al.*, 2004; Yu *et al.*, 2004) have shown ezrin to be an important promoter and regulator of metastasis. However, a central question remains about the steps at which ezrin is involved along the metastatic cascade.

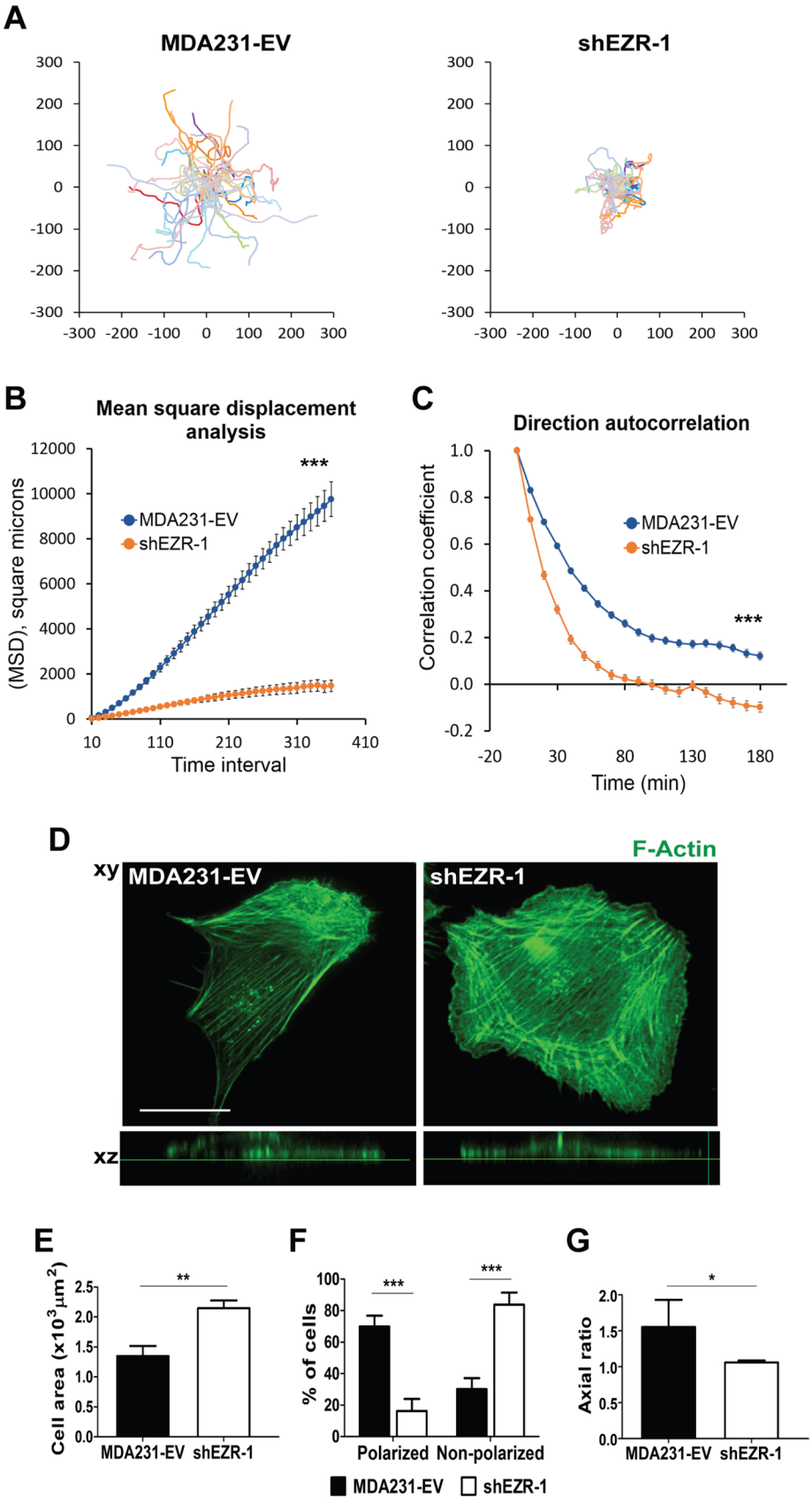

FIGURE 5: Ezrin is required for directional cell migration and front–rear polarization. (A) MDA231-EV and ezrin-depleted (shEZR-1) cells were plated sparsely onto collagen I–coated eight-well Ibidi dishes and analyzed by time-lapse microscopy for 18 h. Cell trajectory data were generated using MetaMorph software and plotted using GraphPad Prism software. MSD (B) and direction autocorrelation (C) analyses were carried out using the open source program DiPer. (D) Representative images of MDA231-EV and shEZR-1 cells stained for F-actin using Alexa 488–phalloidin. The *xz*- planes (bottom) show the relative flatness of the cells. A minimum of 30 cells per line were analyzed. (E) Cell areas were calculated by tracing individual cell outlines using MetaMorph software. (F) The percentage of polarized and nonpolarized cells. Polarized cells were defined as cells that displayed stress fibers aligned along the front–rear axis. (G) The axial ratio, defined as the ratio of the long axis to the short axis of the cell, calculated using F-actin–stained confocal images of cells. Data represent means ± SE (B, C) or + SD (E–G) of three independent experiments. *$p < 0.05$ and **$p < 0.01$ by unpaired *t* test (E, G); ***$p < 0.001$ by linear regression analysis (B), or unpaired *t* test from 10 to 180 min (C), or two-way ANOVA (F). Scale bar, 15 µm.

Our transendothelial migration results support a potential role of ezrin in seeding of metastatic cells at the target organ site. To test this notion, we intravenously injected a 50:50 mixture of control and ezrin-deficient cells labeled with orange and green cell trackers, respectively, into immune-deficient Rag2$^{-/-}$ γc$^{-/-}$ mice. Mice were killed 1 or 24 h postinjection and lungs excised, fixed, and imaged directly by spinning disk fluorescence microscopy. After 1 h, the cell types were present in the lungs in equal proportions (Figure 8A). However, after 24 h, the proportion of ezrin-deficient cells remaining in the lung was reduced to 30 ± 2% of the total cell population (Figure 8A). We next assessed the effect of ezrin depletion on longer-term lung colonization events. To this end, we injected GFP-positive control or ezrin-deficient cells intravenously into mice and harvested lung tissues 3 wk postinjection. Lungs were imaged using biophotonics to quantify the number of GFP-positive tumor nodules and total tumor load. As shown in Figure 8B, ezrin depletion significantly inhibited the number of tumor colonies, as well as total tumor load in the lungs (Figure 8C). Together these results show that ezrin is required for both initial seeding and longer-term outgrowth of tumor colonies at distant organ sites.

To assess the effects of ezrin depletion on primary tumor growth and spontaneous metastasis, we engrafted GFP-positive MDA231 or ezrin-deficient cells into the number 4 mammary fat pad of mice. Ezrin depletion had no significant effect on primary tumor growth (Figure 8, D and E),

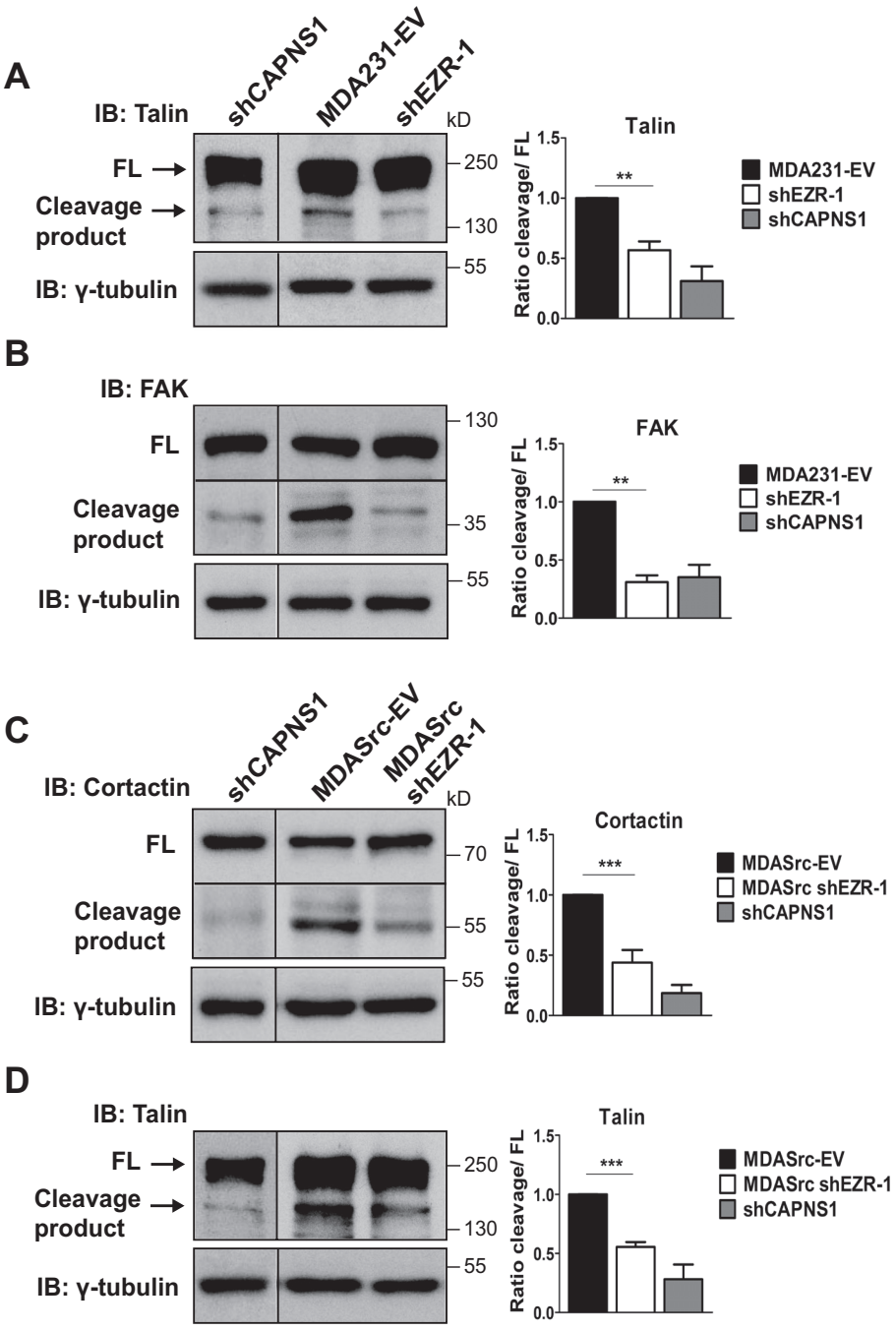

FIGURE 6: Ezrin is required for calpain-mediated cleavage of talin, FAK, and cortactin. Lysates from MDA231-EV and shEZR-1 (A, B) or MDASrc-EV and MDASrc shEZR-1 (C, D) cells were analyzed by immunoblotting using anti-talin, anti-FAK, anti-cortactin, or anti-γ-tubulin antibodies. MDA231 CAPNS1-depleted (shCAPNS1) cell lysates were used to verify the calpain-specific cleavage product for talin, FAK, and cortactin. Quantification of immunoblots was done using densitometry and the results expressed as the fold change in cleavage product to full-length (FL) protein or relative to the control MDA231-EV or MDASrc-EV as described in *Materials and Methods*. Black lines represent merged lanes (vertical) or sections (horizontal) from different areas of the same gel, except for the shCAPNS1 talin lane, which was from a separate gel. Data shown represent means + SD of at least three independent experiments. $^{**}p < 0.01$ and $^{***}p < 0.001$ by one-way ANOVA.

consistent with a metastasis-specific function of this molecule. As expected, ezrin depletion markedly reduced the number of lung metastases compared with control mice, as demonstrated by biophotonics imaging (Figure 8F). Taken together, our results show that ezrin is involved in early lung seeding and colonization of metastasized cancer cells but not primary tumor growth.

DISCUSSION

Important features of invasive cancer cells are directional migration and the ability to adhere to and degrade ECM proteins through the formation of FAs and invadopodia. Although ezrin is known to promote migration and invasion, no studies have yet linked ezrin function to FA or invadopodia dynamics. The data reported here, to our knowledge, are the first to show that ezrin is required for proper disassembly and turnover of FA and invadopodia structures. Two cell types were used in this study: parental MDA231 cells for FA dynamics and MDASrc cells for invadopodia, as the latter cell type preferentially form invadopodia over FAs due to ectopic expression of an active Src mutant. Whereas MDA231 cells are capable of forming invadopodia (i.e., through stimulation with EGF; Hu *et al.*, 2011), the Src-induced invadopodia model allows one to interrogate the role of ezrin in invadopodia function downstream of Src. A study by Cortesio *et al.* (2008) using a similar Src-induced invadopodia model with MTLn3 cells showed that calpain depletion inhibits invadopodia turnover downstream of Src, similar to the results presented here. However, when upstream of Src, calpain regulates invadopodia formation, which emphasizes the dual, context-specific roles of calpain in regulating invadopodia function.

Recent evidence suggests that another ERM protein moesin can also affect invadopodia function but in a manner that differs from ezrin. Beaty *et al.* (2014) demonstrated that, unlike ezrin, moesin localizes to invadopodia in MDA231 cells and is important for promoting maturation of invadopodia to proteolytically active structures by recruiting the sodium ion exchanger NHE-1 to invadopodia precursors. This function is specific to moesin, as Beaty *et al.* (2014) showed that depletion of ezrin does not affect the number of mature invadopodia, even though ezrin can also interact with NHE-1 (Denker *et al.*, 2000). These data also indicate that ezrin may not be required for invadopodia formation, as ezrin-depletion did not affect invadopodia numbers in this study. Furthermore, our results suggest that endogenous moesin levels are not sufficient to maintain proper invadopodia disassembly in the absence of ezrin. Thus, despite the high homology between ezrin and moesin, our findings and those of Beaty *et al.* (2014) highlight distinct but complementary roles of these two ERM proteins in invadopodia function.

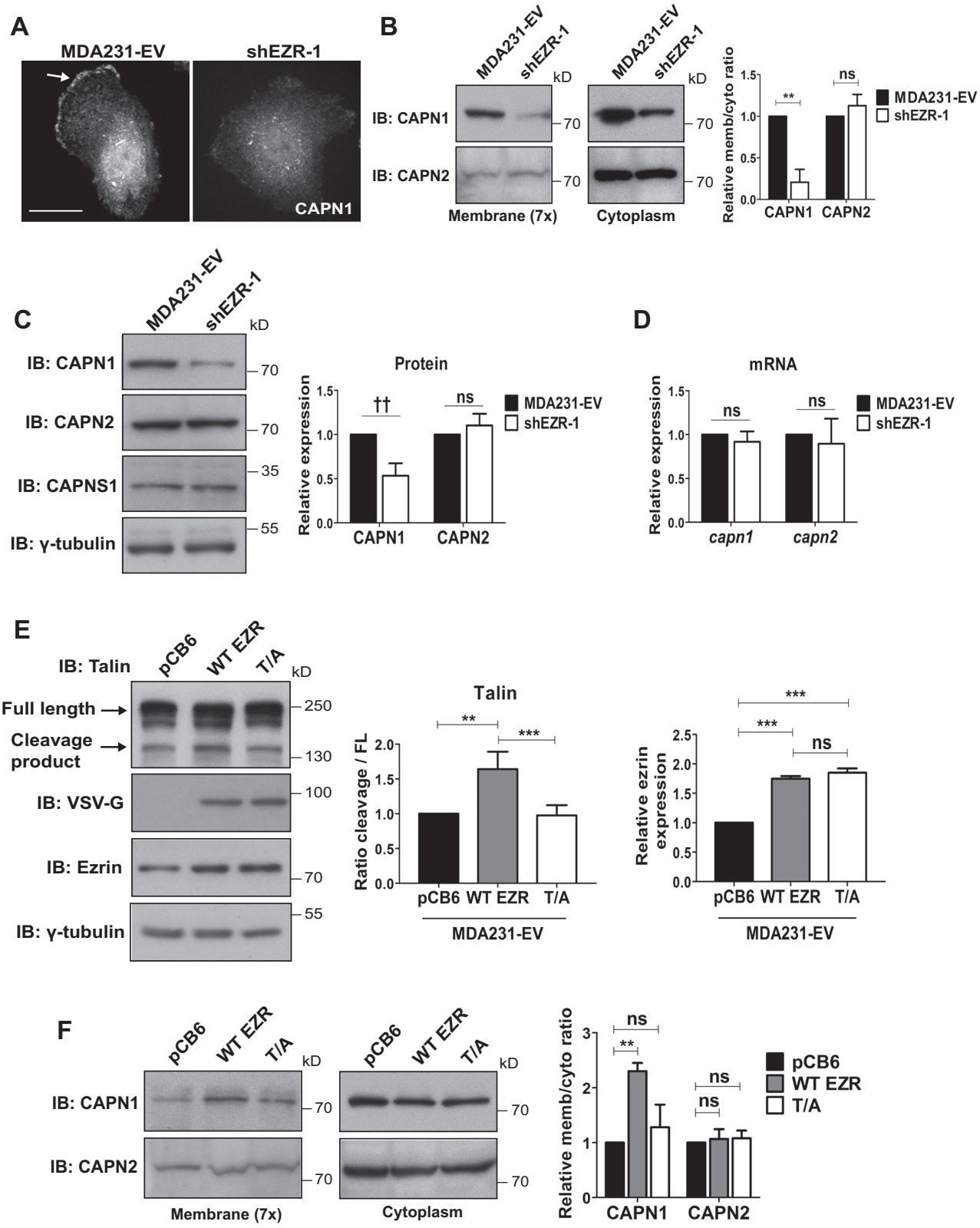

FIGURE 7: Ezrin is required for membrane localization and expression of calpain-1. (A) MDA231-EV and ezrin-depleted cells were stained by immunofluorescence using anti-CAPN1 antibody and images acquired by spinning disk confocal microscopy. Arrow points to membrane localization of CAPN1. Representative images taken at the same *z*-axis plane, near the ventral surface of the cell, for each cell line. A minimum of 30 cells per group were analyzed. (B) Membrane (concentrated sevenfold) and cytoplasmic fractions were immunoblotted with anti-CAPN1 and anti–calpain-2 antibodies. (C) MDA231-EV and shEZR-1 cell lysates were assessed by immunoblotting using anti-CAPN1, anti-calpain-2, and anti- γ-tubulin antibodies. Densitometric analysis was performed to quantify changes in CAPN1 and CAPN2 protein

Phosphorylation of FAK at Y397 induced by cell–ECM adhesion is known to trigger downstream signaling events that lead to adhesion disassembly (Webb *et al.*, 2004; Hamadi *et al.*, 2009), and ezrin is known to interact with FAK (Poullet *et al.*, 2001). However, our data suggest potential defects in these signaling events, as increased phosphorylation of FAK after ezrin depletion is associated with impaired FA turnover.

Regulation of adhesion dynamics is also important in cell directionality. Multiple studies have linked defects in adhesion turnover to a loss of directional migration (Grande-Garcia *et al.*, 2007; Chaki *et al.*, 2013). In our study, ezrin depletion markedly increased the tendency of cells to change direction, an indication that these cells could not maintain a stable polarized morphology with distinct leading and trailing edges. Of interest, cancer cells that exhibit random migration have been linked to tumor progression (Weiger *et al.*, 2013). Furthermore, this characteristic is postulated to be an advantage for cancer cells, as a more exploratory migration phenotype can increase the likelihood of engaging blood or lymphatic vessels for intravasation (Kline *et al.*, 2013).

RhoGTPases are also important for directional motility (Petrie *et al.*, 2009), as well as adhesion dynamics. For instance, Rac activity is associated with lamellipodia and FA formation at the leading edge of the cell, and Rho-dependent actomyosin contractions result in FA maturation and subsequent formation of stress fibers that align in the direction of migration (Rottner *et al.*, 1999; Zaidel-Bar *et al.*, 2003). Our data suggest that Rho activity may not be affected by ezrin depletion, as ezrin-depleted cells form disorganized stress fibers, indicative of a loss of front–rear cell polarity, and display larger, more-elongated adhesions, in contrast to the shorter adhesions characteristic of disrupted Rho function (Rottner *et al.*, 1999; Geiger and Bershadsky, 2001). We also did not observe any defects in FA assembly, implying that Rac activity is not being affected. Because activated ezrin is known to preferentially activate cdc42 to promote directional migration (Prag *et al.*, 2007), depletion of ezrin would therefore be expected to result in a loss of directional persistence. However, cdc42 and Rac regulate the formation of invadopodia (Nakahara *et al.*, 2003), and since invadopodia assembly was not impaired in this study, it is possible that ezrin deficiency is not significantly affecting RhoGTPase activity based on the functional readouts presented here. Nevertheless, our results support the notion that ezrin may regulate directional motility a least in part by promoting adhesion turnover. Despite an increase in the number of invadopodia, the invasive capacity of ezrin-depleted cells was still significantly impaired. This result is consistent with the notion that the ability of cancer cells to form invadopodia alone is not sufficient for invasion to occur, and perturbed FA dynamics can also affect invasion by impeding cellular migration (Chan *et al.*, 2009).

Given that ezrin depletion alters both FA and invadopodia disassembly and that calpain is a known regulator of FA/invadopodia turnover, we hypothesized that ezrin may affect calpain activity. In this study, we show that ezrin depletion inhibits calpain-mediated cleavage of talin, FAK, and cortactin. Furthermore, we demonstrate that a threonine-to-alanine mutation of residue 567 on ezrin hinders calpain cleavage of talin, suggesting that the fully open conformation of ezrin is important for calpain function. Further analysis revealed that CAPN1 but not CAPN2 protein levels were reduced upon ezrin depletion Thus not only is the open and active conformation of ezrin important for calpain-1 activity, but its presence within cancer cells is also required to maintain proper calpain-1 protein expression. These results are intriguing and are consistent with a newly identified role of ezrin in regulating the translation of proteins relevant for metastasis to specific subcellular locations (Briggs *et al.*, 2012). It is also possible that ezrin stabilizes calpain-1 protein from proteasome degradation, as described for Met (Zaarour *et al.*, 2012) and c-Myc (Chuan *et al.*, 2010).

The differential regulation of calpain-1 versus calpain-2 by ezrin is also intriguing since both isoforms are expressed in MDA231 cells and have similar functions. Calpain-2 is the predominant isoform linked to adhesion turnover at the cell rear and is therefore necessary for promoting tail retraction (Glading *et al.*, 2000; Franco *et al.*, 2004), whereas calpain-1 activity is primarily associated with adhesion assembly and disassembly at the leading edge of polarized cells (Glading *et al.*, 2002; Satish *et al.*, 2005). Many studies have also attributed calpain-2 activity to invadopodia/podosome dynamics. For example, calpain-2 cleavage of talin at the adhesion sites within podosome structures is required for their turnover (Calle *et al.*, 2006). In addition, calpain-2-mediated cleavage of the phosphatase PTP1B can regulate Src activity as well as proteolytic cleavage of cortactin, the latter being important for promoting invadopodia disassembly downstream of Src (Cortesio *et al.*, 2008). Our results suggest that calpain-1 also plays a role in invadopodia dynamics and demonstrate that while ezrin has been characteristically known as a substrate of calpain-1, it can also function as an upstream regulator of calpain-1 activity and expression (Figure 9). In support of this notion, a study by Youn *et al.* (2009) showed ezrin to act upstream of a calpain-specific signaling cascade leading to nitric oxide production.

To gain a comprehensive understanding of the function of ezrin as a metastasis-associated protein, it is necessary to identify the steps along the metastatic cascade at which ezrin is involved. Our in vitro data point to a role for ezrin in the intricate regulation of invasion through the extracellular matrix and in transendothelial migration. Our in vivo results suggest that ezrin is mainly important for late-stage disease, including distant organ seeding and longer-term colonization, as ezrin depletion did not attenuate primary tumor growth. These data are consistent with previous reports

expression relative to MDA231-EV cells. (D) Quantitative real-time PCR was performed to analyze *capn1* and *capn2* mRNA levels from MDA231-EV and ezrin-depleted cells. (E) MDA231-EV cells were transiently transfected with empty vector control (pCB6), wild-type ezrin (WT EZR), or a mutant form of ezrin with alanine substituted for threonine at residue 567 (T/A). Both WT EZR and T/A were tagged at the N-terminus with VSV-G. Cell lysates were analyzed by Western blotting using anti-ezrin, anti-talin, anti–VSV-G, or anti–γ-tubulin antibodies. Densitometry was performed to assess the fold change in talin cleavage relative to full-length protein, as well as the amount of exogenous ezrin present in WT and T/A transfected cells relative to pCB6. (F) Membrane (concentrated sevenfold) and cytoplasmic fractions from pCB6, WT EZR, and T/A-overexpressing MDA231-EV cells were immunoblotted for anti-CAPN1 and anti-calpain-2 antibodies. (B, F) Membrane-to-cytoplasmic (memb/cyto) ratios of CAPN1 and CAPN2 were assessed by densitometric analysis of immunoblots from the same exposure and normalized to control MDA231-EV or pCB6. For each protein, membrane and cytoplasmic lysates were run on the same gel. Data shown represent means + SD of three independent experiments. $^{**}p < 0.01$ and $^{***}p < 0.001$ by one-sample *t* test (B), or one-way ANOVA with Tukey's multiple comparison test (E, F). $^{\dagger\dagger}p < 0.002$ by one-sample *t* test (C). Scale bars, 15 μm; ns, not significant.

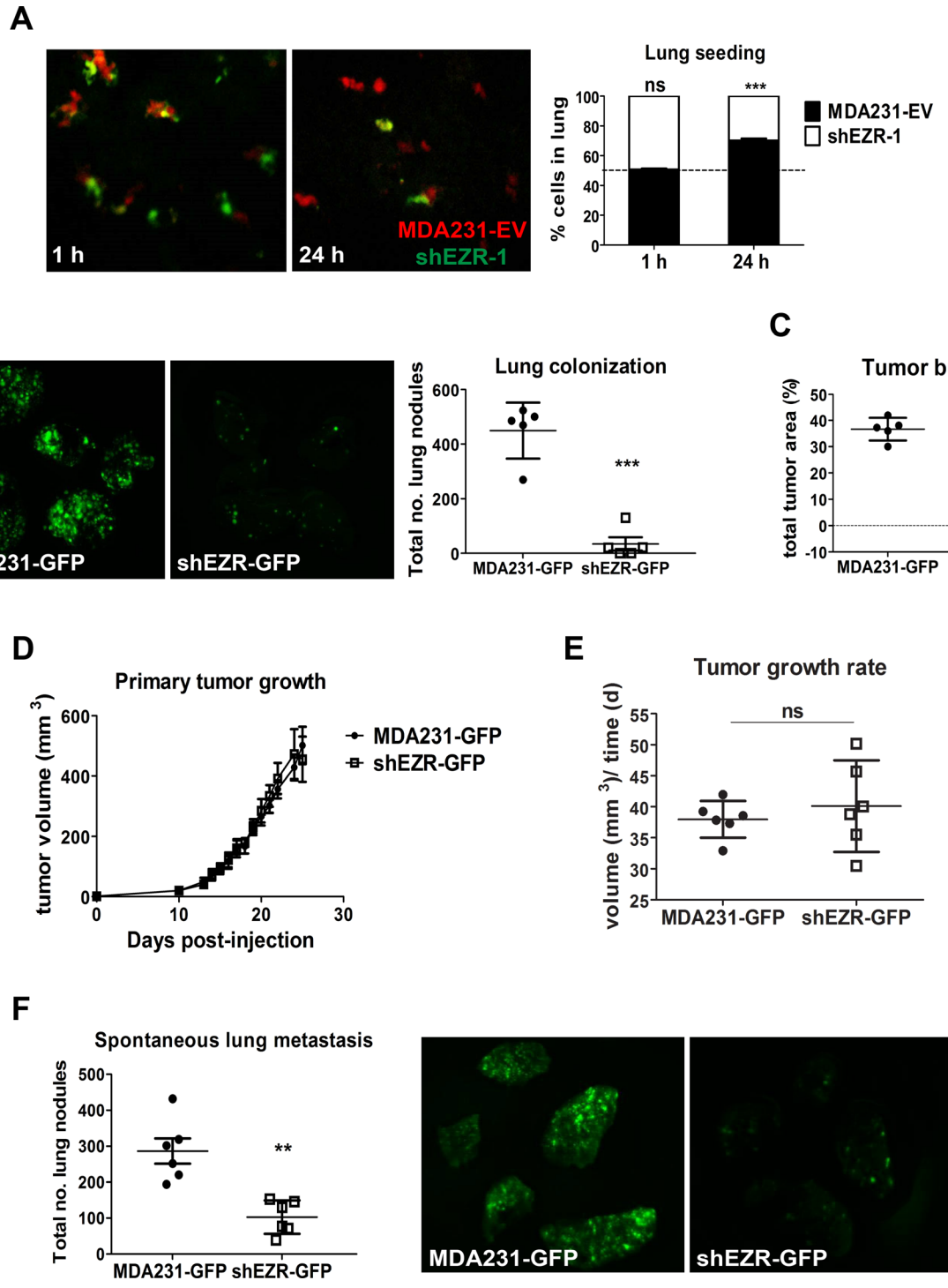

FIGURE 8: Ezrin is required for early lung seeding events and colonization but not primary tumor growth. (A) MDA231-EV (red) and ezrin-depleted (shEZR-1) cells (green) were mixed in equal proportions and injected into the tail veins of mice. Representative confocal images of lungs harvested 1 or 24 h postinjection. Histogram denotes the relative proportion of cells at the indicated times (five mice per group per time point). (B) Representative biophotonic images of lungs harvested 3 wk after tail vein injection of GFP-labeled MDA231 and ezrin-depleted cells (five mice per group). The total number of lung colonies was quantified using ImagePro Plus 6.0 software. (C) Tumor burden evaluated as the percentage of GFP-positive pixel areas relative to total lung area. (D) Primary tumor volumes measured and calculated as described in *Materials and Methods* (six mice per group). (E) Tumor growth rates generated from the slopes of tumor growth curves. (F) Representative biophotonics images of lungs harvested 24 d after tumor injection (six mice per group). Data shown represent means ± SD. $^{**}p < 0.01$ by Mann–Whitney *U* test (F) and $^{***}p < 0.001$ by unpaired *t* test (A) or Mann–Whitney *U* test (B, C).

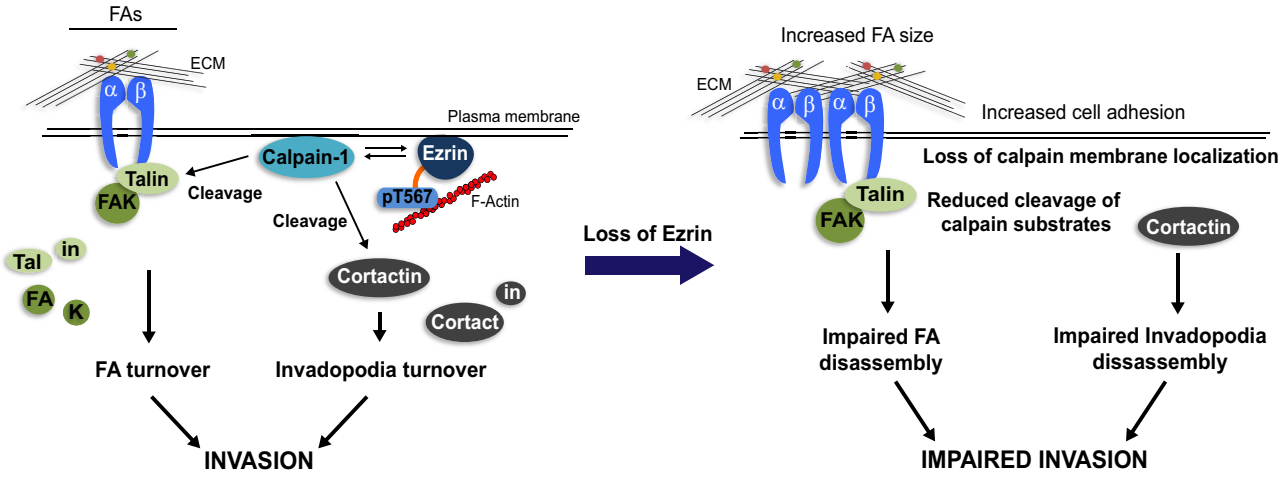

FIGURE 9: Model for ezrin regulation of calpain-1 and FA/invadopodia dynamics. Plasma membrane localization of ezrin and calpain-1 is important for their function. By facilitating anchorage of calpain-1 to the cell periphery, ezrin promotes FA and invadopodia turnover by placing calpain-1 in close proximity to its substrates—talin, FAK, and cortactin. Depleting ezrin expression (by shRNA) or inhibiting its open active conformation (by T/A mutation) perturbs calpain-1–membrane linkage and therefore cleavage of the calpain substrates necessary for efficient FA/invadopodia disassembly, resulting in impaired cancer cell invasion.

showing that ezrin promotes early metastatic survival signaling through activation of the phosphoinositide 3-kinase/Akt pathway (Khanna *et al.*, 2004; Chen *et al.*, 2011).

In summary, our findings reveal a novel regulatory role for ezrin in promoting proper FA and invadopodia turnover by regulating calpain-1 membrane localization and activity toward key components of FAs and invadopodia. By dissecting the various steps of the metastatic cascade, we show that ezrin function is indeed required for specific aspects of tumor cell dissemination and thus begin to understand the complexity of ezrin as a metastasis-associated protein. Future investigation will elucidate the precise regulation of calpain-1 activity by ezrin and whether calpain-1 is required for ezrin-mediated metastasis. Information from this study will provide important mechanistic insight in evaluating ezrin as a potential prognostic marker of metastatic relapse in breast cancer patients.

MATERIALS AND METHODS

Antibodies and reagents

Rabbit anti–β1 integrin, goat anti-CAPN1, and rabbit anti-FAK were from Santa Cruz Biotechnology (Dallas, TX). Rabbit anti-ezrin was purchased from Cell Signaling (Beverly, MA). Rabbit anti–phospho-Y397 FAK and mouse anti-paxillin were from BD Transduction Labs (Mississauga, Canada). Mouse anti-cortactin was purchased from EMD Millipore (Etobicoke, Canada). Mouse anti–γ-tubulin, mouse anti-moesin, mouse anti-vinculin, mouse anti-talin, and rabbit anti-zyxin were purchased from Sigma-Aldrich (Oakville, Canada). Rabbit anti–calpain-2, which recognizes both CAPN2 and CAPNS1, was provided by P. Greer (Queen's University, Kingston, Canada; Arthur *et al.*, 2000). Transwell chambers (8-μm pore size) were obtained from Corning (Mississauga, Canada). Eight-well chamber slides were purchased from LabTek (Mississauga, Canada). μ-Slide VI, 35-mm μ-Dish, and eight-well μ-Slides were from Ibidi (Madison, WI). Alexa Fluor reagents and cell trackers were obtained from Life Technologies (Burlington, Canada). Growth factor–reduced Matrigel and rat-tail collagen I were purchased from BD Biosciences (Mississauga, Canada). Fibronectin, gelatin, and puromycin were from Sigma-Aldrich.

Cell culture, transfection, and constructs

MDA-MB-231 (MDA231) human breast cancer cells were provided by P. Siegel (McGill University, Montreal, Canada). MDA231 cells stably expressing an avian Src Y527F mutant (referred to as MDASrc) were obtained from A. Mak (Queen's University; Hu *et al.*, 2011), and MDASrc cells were transduced with either EV or ezrin shRNA as will be described. HEK293T cells were obtained from the American Type Culture Collection (Manassas, VA). All cell lines were maintained in DMEM supplemented with 10% fetal bovine serum (FBS; Sigma-Aldrich) at 37°C in a humidified atmosphere with 5% CO_2. Transient transfections were performed using FugeneHD reagent (Promega, Madison, WI) according to the manufacturer's protocol. RFP-zyxin was obtained from Addgene (plasmid 26720; Cambridge, MA). GFP-cortactin was provided by A. Craig (Queen's University). The pCB6 empty vector and WT and T/A ezrin constructs were a kind gift from M. Arpin (Curie Institute, Paris, France). All cell lines were routinely tested for mycoplasma using the Lookout Mycoplasma PCR Detection Kit (Sigma-Aldrich).

Ezrin and calpain knockdown

Human *EZR*- and *capns1*-specific shRNA and EV control pLKO.1 lentiviral vectors were purchased from GE Healthcare Dharmacon. Viral particles were prepared by transfecting HEK293T cells with psPAX2 packaging, pMD2.G envelope, and pLKO.1 EV or ezrin shRNA vectors using Lipofectamine 2000 transfection reagent (Life Technologies), as per the manufacturer's protocol. Virus-containing supernatant was collected and passed through 0.45-μm syringe filters before addition to target cells. Stably transfected cells were selected in 4 μg/ml puromycin. Knockdown of ezrin protein was confirmed by immunoblot.

Immunoblotting

Whole-cell lysates were prepared as follows. Cells were rinsed twice in ice-cold phosphate-buffered saline (PBS) and lysed in 2× Laemmli buffer. Total protein concentrations were determined using the DC Protein Assay (Bio-Rad, Mississauga, Canada). From 10 to 30 μg of protein was separated by SDS–PAGE and transferred to 0.45 μm

polyvinylidene fluoride membranes (EMD Millipore). Membranes were blocked in 5% nonfat dry milk in 1× Tris-buffered saline/0.1% Tween-20 and then probed with the indicated antibodies. Primary antibodies were detected with horseradish peroxidase–bound secondary antibodies and Pierce ECL Plus Western Blotting Substrate (Life Technologies). Densitometry was performed using ImageJ software (National Institutes of Health, Bethesda, MD).

Calpain substrate cleavage analysis

Quantitative assessment of the levels of calpain-mediated cleavage of talin, FAK, and cortactin was performed by calculating the ratio of the cleavage product to the full-length protein based on densitometry readings from the same gel. Different autoradiographic exposures were used for optimal detection of the full-length and cleaved proteins. The molecular weights of the major calpain-specific cleavage products for talin, FAK, and cortactin were used for the analyses (~200, ~35, and ~55 kDa, respectively) as previously described (Dourdin *et al.*, 2001; Perrin *et al.*, 2006; Chan *et al.*, 2010).

Cytosol/membrane fractionation

Subcellular fractionation was performed as follows. Cells from confluent cultures in 100-mm dishes were rinsed twice in cold PBS. Cells were scraped off in 350 µl of cell fractionation buffer containing 20 mM 4-(2-hydroxyethyl)-1-piperazineethanesulfonic acid (HEPES; pH 7.4), 1 mM EDTA, 1 mM ethylene glycol tetraacetic acid, 10 mM KCl, 1.5 mM $MgCl_2$, 250 mM sucrose, and a cocktail of protease/phosphatase inhibitors and then mechanically disrupted with a 27-gauge needle (10 times). Homogenates were clarified by centrifugation at 600 × *g*. The supernatant was then subjected to a 60-min centrifugation at 100,000 × *g*. The resulting supernatant (cytosolic fraction) was supplemented with 6× Laemmli buffer. Pellets (membrane fraction) were solubilized in 50 µl of 1× Laemmli buffer. Samples were separated by SDS–PAGE and analyzed by immunoblotting. Membrane-to-cytoplasmic ratios of CAPN1 and CAPN2 were assessed by densitometric analysis of immunoblots from the same exposure and normalized to control MDA231-EV or pCB6. For each protein, membrane and cytoplasmic lysates were run on the same gel.

Immunofluorescence

Cells (1.7×10^4) were seeded onto collagen I–coated Ibidi µ-Slides (VI), fixed in 2% paraformaldehyde, permeabilized with 0.2% Triton X-100, and blocked in 3% bovine serum albumin (BSA). Cells were then stained with the indicated primary antibodies and appropriate Alexa Fluor 546 or 633 secondary antibodies. For focal adhesion proteins, cells were visualized by total internal reflection fluorescence (TIRF) microscopy using a 63×/1.42 numerical aperture oil objective on an inverted Olympus BX-80 confocal microscope equipped with a multicolor TIRF module and a Hamamatsu electron-multiplying charge-coupled device digital camera (Spectral Applied Research, Richmond Hill, Canada). All other markers were visualized using a 63× oil objective on an inverted Quorum WaveFX-X1 Spinning Disk confocal microscope system (Quorum Technologies, Guelph, Canada). Images were collected through 593/40- or 692/40-nm emission filters. The 16-bit images were aligned and quantified using MetaMorph software (Molecular Devices, Sunnyvale, CA).

Real-time fluorescence microscopy and quantification of FA and invadopodia dynamics

Fluorescence imaging of RFP-zyxin and GFP-cortactin dynamics was performed to detect FA and invadopodia, respectively, using a 40× objective on an inverted Quorum WaveFX-X1 Spinning Disk confocal microscope in a closed system at 37°C and 5% CO_2. The 35-mm µ-dishes (Ibidi) were coated with 10 µg/ml collagen I for 1 h at 37°C. Cells (3.5×10^4) were plated in DMEM/F12 containing 10% FBS and 20 mM HEPES and allowed to adhere for 3 h. Images were captured every 1 min for a minimum of 3 h. Measurements of fluorescence-labeled FA and invadopodia spots and calculations of assembly and disassembly rate constants were performed as described previously (Chan *et al.*, 2007, 2009). At least 40 FAs or invadopodia spots were analyzed per experiment.

Real-time cell migration assays

Cells (1.5×10^4) were seeded sparsely onto collagen I–coated eight-well µ-slides in DMEM/F12 containing 10% FBS and 20 mM HEPES and incubated at 37°C for 3 h. Cells were then imaged every 10 min for 18 h using a 10× objective on an inverted Quorum WaveFX-X1 Spinning Disk confocal microscope with bright-field illumination in a closed system at 37°C and 5% CO_2. Individual cells were tracked using MetaMorph software. Cell tracks were graphed using Excel. A minimum of 50 cells were analyzed per experiment.

Immunoprecipitation

Cells were grown to 85% confluence and lysed in a buffer containing 20 mM Tris (pH 7.5), 150 mM NaCl, 1 mM EDTA, 1% (wt/vol) NP-40, and 1× Halt protease/phosphatase inhibitor cocktail (Life Technologies). Lysates were incubated overnight with Gammabind G–Sepharose beads plus antibody (GE Healthcare Dharmacon). Immunoprecipitates were subsequently analyzed by immunoblot as described.

Extracellular matrix degradation and gelatin zymogram assays

Cells (1×10^4) were plated onto gelatin-coated coverslips containing a layer of fluorescein isothiocyanate (FITC)–conjugated fibronectin prepared as previously described (Webb *et al.*, 2007). Cells were incubated for 72 h for consistency of ECM degradation (Furmaniak-Kazmierczak *et al.*, 2007) and subsequently fixed in 2% paraformaldehyde and stained for F-actin using Alexa Fluor–phalloidin 594. Images were acquired using spinning disk confocal microscopy. In this assay, proteolysis of the FITC-fibronectin results in the appearance of nonfluorescent areas. Owing to the strong migratory phenotype of MDASrc cells, extensive areas of ECM degradation not associated with actin-rich structures were visible (Figure 4B). Therefore the total area of degradation spots from at least 10 fields per experiment was quantified using ImagePro Plus 6.0 software (Media Cybernetics, Rockville, MD). MMP activity was assessed using gelatin zymography, as described previously (Hauck *et al.*, 2002). Briefly, conditioned medium from MDASrc and MDASrc shEZR cells was collected for 48 h and resolved in nonreducing gels containing 0.2% (wt/vol) gelatin. Areas of gelatin degradation bands were visualized using 0.4% Coomassie blue staining.

Cell adhesion assays

Cells (5×10^4) were seeded in quadruplicate onto 5 µg/ml collagen I– or 3% BSA–coated wells (as a negative control) in a 96-well plate and allowed to adhere for 30 min at 37°C. Wells were then washed several times with PBS to remove any unbound cells. Cells were then fixed and stained using a 0.4% solution of toluidine blue O in 4% paraformaldehyde/PBS for 15 min at room temperature. Adhesion was measured colorimetrically at 570 nm.

Invasion assays

Transwell inserts were coated with 100 µl of 20% Matrigel (diluted in serum-free DMEM) and incubated at 37°C for 1 h to allow the

Matrigel to gel. Cells were trypsinized and resuspended in serum-free DMEM. A 100-µl amount containing 5×10^4 cells was seeded into the upper chamber, and 500 µl of DMEM plus 10% FBS was added to the lower chamber as a chemoattractant. Cells were allowed to invade for 18 h, after which Transwell membranes were fixed in 2% paraformaldehyde and nuclei stained using 4′,6-diamidino-2-phenylindole (DAPI). Invaded cells were visualized with a BX51 System Microscope (Olympus, Toronto, Canada) and images acquired using QCapture Pro 5.0 software (QImaging, Surrey, Canada). Invaded cells were quantified using ImagePro Plus 6.0 software.

Transendothelial migration assays

Human umbilical vein endothelial cells (5×10^4) were seeded on collagen I–coated Transwell inserts and adhered for 18 h. Tumor cells cultured on a 100-mm dish were loaded with a green cell tracker and seeded (1×10^4) on top of the endothelial monolayer. Cells were allowed to migrate for 6 h, after which, Transwell membranes were fixed in 2% paraformaldehyde and nuclei stained using DAPI. Migrated tumor cells were visualized with a BX51 System Microscope and images acquired using QCapture Pro 5.0 software. Migrated tumor cells were quantified using ImagePro Plus 6.0 software.

Real-time PCR

Total RNA was purified from MDA231-EV and shEZR-1 cells using TRIzol reagent according to the manufacturer's instructions (Life Technologies). cDNA was synthesized from 1 µg of total RNA using the iScript Select cDNA Synthesis Kit with random primers (Bio-Rad). Samples were incubated at 16°C for 30 min, followed by 42°C for 30 min and 85°C for 5 min. The levels of *capn1* and *capn2* were detected using the iQ SYBR Green Supermix Kit on the iQ5 Multi-Color Real-Time PCR Detection System (Bio-Rad). Primer sequences were as follows. CAPN1: forward, 5′-AACAAGGAGGG-CGACTTCGT-3′; reverse, 5′-CTTCCGGAAGATGGACAGGT-3′. CAPN2: forward, 5′-AGGCATACGCCAAGATCAAC-3′; reverse, 5′-GGATGCGGATCAGTTTCTGT-3′. Glyceraldehyde-3-phosphate dehydrogenase: forward, 5′-GAGTCAACGGATTTGGTCGTAT-3′; reverse, 5′-AGTCTTCTGGGTGGCAGTGAT-3′. Conditions of the thermal cycling were initial denaturation for 3 min at 95°C, followed by 50 cycles of denaturation for 15 s at 95°C and annealing/extension for 45 s at 55°C. Differences in the expression levels of genes were determined by calculating the fold change in expression (2^{-ddCT}). Values are expressed relative to control MDA231-EV. All primer sequences were used in previous publications (Ueyama *et al.*, 1998; Nuzzi *et al.*, 2007).

In vivo studies

Mice were housed in the Queen's Animal Care Facility, and procedures were carried out according to the guidelines of the Canadian Council on Animal Care, with the approval of the institutional animal care committee. For the tumor xenograft studies, GFP-labeled MDA231control (empty vector) or ezrin-depleted cells (1×10^6 in 50 µl of 50% Matrigel) were injected into the mammary fat pad of Rag2$^{-/-}$ $\gamma c^{-/-}$ mice, as described previously (Elliott *et al.*, 2005). At 25 d postinjection, primary tumors and lungs were excised and fixed in 4% paraformaldehyde/PBS. Measurements of tumor volume, histological processing and assessments, and analysis of local invasion and metastasis were performed as described previously (Mak *et al.*, 2012). For assessment of GFP-expressing metastatic nodules, lungs were dissected and analyzed by biophotonics. Images were captured using a Hamamatsu ORCA-ER digital camera. For the lung-seeding assays, control and ezrin-deficient cells were preloaded with Orange-CMTMR and calcein cell trackers, respectively. Cells were mixed in equal proportion and injected into the tail veins of mice (1×10^6 total in 200 µl of PBS), as previously reported (Pinner and Sahai, 2008). Lungs were harvested 1 or 24 h postinjection, fixed in 4% paraformaldehyde/PBS, and directly imaged using a 10× objective on a spinning disk confocal microscope. At least 10 fields were imaged per lung, with a minimum of 150 cells counted.

Statistical analysis

All statistical analyses were performed using GraphPad Prism Software, version 5.0. All error bars represent SD from the mean unless otherwise indicated. The *p* values were calculated by unpaired or one-sample *t* test or one-way or two-way analysis of variance (ANOVA). Lung metastases data sets were analyzed by a Mann–Whitney *U* test. Specific conditions and *p* values for each test are described in the figure legends.

ACKNOWLEDGMENTS

We thank C. Schick and E. Furmaniak-Kazmierczak for technical assistance. J. Macleod provided aliquots of the shCAPNS1 construct. A. Day provided statistical advice. We also thank the lab of A. Craig for expertise and assistance with our real-time PCR studies and R. Gorelik for advice on our analysis of directional persistence. This work is supported by a grant from the Canadian Institutes of Health Research (MOP-102644) to B.E.E. V.H. is the recipient of a Canadian Breast Cancer Foundation Doctoral Fellowship. A.G. is supported by a CIHR Postdoctoral Fellowship. A.S. is the recipient of an Ontario Graduate Scholarship. V.H., A.S., and A.G. held scholarships from the Terry Fox Foundation Training Program in Transdisciplinary Cancer Research in partnership with the Canadian Institutes of Health Research.

REFERENCES

Arthur JA, Elce JS, Hegadorn C, Williams K, Greer PA (2000). Disruption of the murine calpain small subunity gene, Capn4: calpain is essential for embryonic development but not for cell growth and division. Mol Cell Biol 20, 4474–4481.

Badowski C, Pawlak G, Grichine A, Chabadel A, Oddou C, Jurdic P, Pfaff M, Albiges-Rizo C, Block MR (2008). Paxillin phosphorylation controls invadopodia/podosomes spatiotemporal organization. Mol Biol Cell 19, 633–645.

Beaty BT, Wang Y, Bravo-Cordero JJ, Sharma VP, Miskolci V, Hodgson L, Condeelis J (2014). Talin regulates moesin-NHE-1 recruitment to invadopodia and promotes mammary tumor metastasis. J Cell Biol 205, 737–751.

Bretscher A, Edwards K, Fehon RG (2002). ERM proteins and merlin: integrators at the cell cortex. Nat Rev Mol Cell Biol 3, 586–599.

Briggs JW, Ren L, Nguyen R, Chakrabarti K, Cassavaugh J, Rahim S, Bulut G, Zhou M, Veenstra TD, Chen Q, *et al.* (2012). The ezrin metastatic phenotype is associated with the initiation of protein translation. Neoplasia 14, 297–310.

Bruce B, Khanna G, Ren L, Landberg G, Jirstrom K, Powell C, Borczuk A, Keller ET, Wojno KJ, Meltzer P, *et al.* (2007). Expression of the cytoskeleton linker protein ezrin in human cancers. Clin Exp Metastasis 24, 69–78.

Calle Y, Carragher NO, Thrasher AJ, Jones GE (2006). Inhibition of calpain stabilises podosomes and impairs dendritic cell motility. J Cell Sci 119, 2375–2385.

Carneiro A, Bendahl PO, Akerman M, Domanski HA, Rydholm A, Engellau J, Nilbert M (2011). Ezrin expression predicts local recurrence and development of metastases in soft tissue sarcomas. J Clin Pathol 64, 689–694.

Carragher NO, Frame MC (2004). Focal adhesion and actin dynamics, a place where kinases and proteases meet to promote invasion. Trends Cell Biol 14, 241–249.

Chaki SP, Barhoumi R, Berginski ME, Sreenivasappa H, Trache A, Gomez SM, Rivera GM (2013). Nck enables directional cell migration through the coordination of polarized membrane protrusion with adhesion dynamics. J Cell Sci 126, 1637–1649.

Chan KT, Bennin DA, Huttenlocher A (2010). Regulation of adhesion dynamics by calpain-mediated proteolysis of focal adhesion kinase (FAK). J Biol Chem 285, 11418–11426.
Chan KT, Cortesio CL, Huttenlocher A (2007). Integrins in cell migration. Methods Enzymol 426, 47–67.
Chan KT, Cortesio CL, Huttenlocher A (2009). FAK alters invadopodia and focal adhesion composition and dynamics to regulate breast cancer invasion. J Cell Biol 185, 357–370.
Chen Q, Zhang XH, Massague J (2011). Macrophage binding to receptor VCAM-1 transmits survival signals in breast cancer cells that invade the lungs. Cancer Cell 20, 538–549.
Chuan YC, Iglesias-Gato D, Fernandez-Perez L, Cedazo-Minguez A, Pang ST, Norstedt G, Pousette A, Flores-Morales A (2010). Ezrin mediates c-Myc actions in prostate cancer cell invasion. Oncogene 29, 1531–1542.
Cortesio CL, Chan KT, Perrin BJ, Burton NO, Zhang S, Zhang ZY, Huttenlocher A (2008). Calpain 2 and PTP1B function in a novel pathway with Src to regulate invadopodia dynamics and breast cancer cell invasion. J Cell Biol 180, 957–971.
Deakin NO, Turner CE (2011). Distinct roles for paxillin and Hic-5 in regulating breast cancer cell morphology, invasion, and metastasis. Mol Biol Cell 22, 327–341.
Denker SP, Huang DC, Orlowski J, Furthmayr H, Barber DL (2000). Direct binding of the Na–H exchanger NHE1 to ERM proteins regulates the cortical cytoskeleton and cell shape independently of H(+) translocation. Mol Cell 6, 1425–1436.
Dewitt S, Hallett M (2007). Leukocyte membrane "expansion": a central mechanism for leukocyte extravasation. J Leukocyte Biol 81, 1160–1164.
Dourdin N, Bhatt AK, Dutt P, Greer PA, Arthur JS, Elce JS, Huttenlocher A (2001). Reduced cell migration and disruption of the actin cytoskeleton in calpain-deficient embryonic fibroblasts. J Biol Chem 276, 48382–48388.
Elliott BE, Meens JA, SenGupta SK, Louvard D, Arpin M (2005). The membrane cytoskeletal crosslinker ezrin is required for metastasis of breast carcinoma cells. Breast Cancer Res: BCR 7, R365–R373.
Elliott BE, Qiao H, Louvard D, Arpin M (2004). Co-operative effect of c-Src and ezrin in deregulation of cell-cell contacts and scattering of mammary carcinoma cells. J Cell Biochem 92, 16–28.
Elzagheid A, Korkeila E, Bendardaf R, Buhmeida A, Heikkila S, Vaheri A, Syrjanen K, Pyrhonen S, Carpen O (2008). Intense cytoplasmic ezrin immunoreactivity predicts poor survival in colorectal cancer. Hum Pathol 39, 1737–1743.
Franco SJ, Rodgers MA, Perrin BJ, Han J, Bennin DA, Critchley DR, Huttenlocher A (2004). Calpain-mediated proteolysis of talin regulates adhesion dynamics. Nat Cell Biol 6, 977–983.
Furmaniak-Kazmierczak E, Crawley SW, Carter RL, Maurice DH, Cote GP (2007). Formation of extracellular matrix-digesting invadopodia by primary aortic smooth muscle cells. Circ Res 100, 1328–1336.
Gautreau A, Louvard D, Arpin M (2000). Morphogenic effects of ezrin require a phosphorylation-induced transition from oligomers to monomers at the plasma membrane. J Cell Biol 150, 193–203.
Gavazzi I, Nermut MV, Marchisio PC (1989). Ultrastructure and gold-immunolabelling of cell-substratum adhesions (podosomes) in RSV-transformed BHK cells. J Cell Sci 94, 85–99.
Geiger B, Bershadsky A (2001). Assembly and mechanosensory function of focal contacts. Curr Opin Cell Biol 13, 584–592.
Glading A, Chang P, Lauffenburger DA, Wells A (2000). Epidermal growth factor receptor activation of calpain is required for fibroblast motility and occurs via an ERK/MAP kinase signaling pathway. J Biol Chem 275, 2390–2398.
Glading A, Lauffenburger DA, Wells A (2002). Cutting to the chase: calpain proteases in cell motility. Trends Cell Biol 12, 46–54.
Gorelik R, Gautreau A (2014). Quantitative and unbiased analysis of directional persistence in cell migration. Nat Protoc 9, 1931–1943.
Grande-Garcia A, Echarri A, de Rooij J, Alderson NB, Waterman-Storer CM, Valdivielso JM, del Pozo MA (2007). Caveolin-1 regulates cell polarization and directional migration through Src kinase and Rho GTPases. J Cell Biol 177, 683–694.
Hamadi A, Deramaudt TB, Takeda K, Ronde P (2009). Src activation and translocation from focal adhesions to membrane ruffles contribute to formation of new adhesion sites. Cell Mol Life Sci 66, 324–338.
Hauck CR, Hsia DA, Puente XS, Cheresh DA, Schlaepfer DD (2002). FRNK blocks v-Src-stimulated invasion and experimental metastases without effects on cell motility or growth. EMBO J 21, 6289–6302.
Hu J, Mukhopadhyay A, Truesdell P, Chander H, Mukhopadhyay UK, Mak AS, Craig AW (2011). Cdc42-interacting protein 4 is a Src substrate that regulates invadopodia and invasiveness of breast tumors by promoting MT1-MMP endocytosis. J Cell Sci 124, 1739–1751.
Kaverina I, Krylyshkina O, Small JV (1999). Microtubule targeting of substrate contacts promotes their relaxation and dissociation. J Cell Biol 146, 1033–1044.
Khanna C, Wan X, Bose S, Cassaday R, Olomu O, Mendoza A, Yeung C, Gorlick R, Hewitt SM, Helman LJ (2004). The membrane-cytoskeleton linker ezrin is necessary for osteosarcoma metastasis. Nat Med 10, 182–186.
Kline ER, Shupe J, Gilbert-Ross M, Zhou W, Marcus AI (2013). LKB1 represses focal adhesion kinase (FAK) signaling via a FAK-LKB1 complex to regulate FAK site maturation and directional persistence. J Biol Chem 288, 17663–17674.
Kobel M, Langhammer T, Huttelmaier S, Schmitt WD, Kriese K, Dittmer J, Strauss HG, Thomssen C, Hauptmann S (2006). Ezrin expression is related to poor prognosis in FIGO stage I endometrioid carcinomas. Modern Pathol 19, 581–587.
Kopp P, Lammers R, Aepfelbacher M, Woehlke G, Rudel T, Machuy N, Steffen W, Linder S (2006). The kinesin KIF1C and microtubule plus ends regulate podosome dynamics in macrophages. Mol Biol Cell 17, 2811–2823.
Leloup L, Shao H, Bae YH, Deasy B, Stolz D, Roy P, Wells A (2010). m-Calpain activation is regulated by its membrane localization and by its binding to phosphatidylinositol 4,5-bisphosphate. J Biol Chem 285, 33549–33566.
Linder S (2007). The matrix corroded: podosomes and invadopodia in extracellular matrix degradation. Trends Cell Biol 17, 107–117.
Mak H, Naba A, Varma S, Schick C, Day A, SenGupta SK, Arpin M, Elliott BE (2012). Ezrin phosphorylation on tyrosine 477 regulates invasion and metastasis of breast cancer cells. BMC Cancer 12, 82.
Naba A, Reverdy C, Louvard D, Arpin M (2008). Spatial recruitment and activation of the Fes kinase by ezrin promotes HGF-induced cell scattering. EMBO J 27, 38–50.
Nakahara H, Otani T, Sasaki T, Miura Y, Takai Y, Kogo M (2003). Involvement of Cdc42 and Rac small G proteins in invadopodia formation of RPMI7951 cells. Genes Cells 8, 1019–1027.
Nuzzi PA, Senetar MA, Huttenlocher A (2007). Asymmetric localization of calpain 2 during neutrophil chemotaxis. Mol Biol Cell 18, 795–805.
Perrin BJ, Amann KJ, Huttenlocher A (2006). Proteolysis of cortactin by calpain regulates membrane protrusion during cell migration. Mol Biol Cell 17, 239–250.
Petrie RJ, Doyle AD, Yamada KM (2009). Random versus directionally persistent cell migration. Nat Rev Mol Cell Biol 10, 538–549.
Pinner S, Sahai E (2008). PDK1 regulates cancer cell motility by antagonising inhibition of ROCK1 by RhoE. Nat Cell Biol 10, 127–137.
Poullet P, Gautreau A, Kadare G, Girault JA, Louvard D, Arpin M (2001). Ezrin interacts with focal adhesion kinase and induces its activation independently of cell-matrix adhesion. J Biol Chem 276, 37686–37691.
Prag S, Parsons M, Keppler MD, Ameer-Beg SM, Barber P, Hunt J, Beavil AJ, Calvert R, Arpin M, Vojnovic B, Ng T (2007). Activated ezrin promotes cell migration through recruitment of the GEF Dbl to lipid rafts and preferential downstream activation of Cdc42. Mol Biol Cell 18, 2935–2948.
Rottner K, Hall A, Small JV (1999). Interplay between Rac and Rho in the control of substrate contact dynamics. Curr Biol 9, 640–648.
Saotome I, Curto M, McClatchey AI (2004). Ezrin is essential for epithelial organization and villus morphogenesis in the developing intestine. Dev Cell 6, 855–864.
Sarrio D, Rodriguez-Pinilla SM, Dotor A, Calero F, Hardisson D, Palacios J (2006). Abnormal ezrin localization is associated with clinicopathological features in invasive breast carcinomas. Breast Cancer Res Treatment 98, 71–79.
Satish L, Blair HC, Glading A, Wells A (2005). Interferon-inducible protein 9 (CXCL11)-induced cell motility in keratinocytes requires calcium flux-dependent activation of mu-calpain. Mol Cell Biol 25, 1922–1941.
Shao H, Chou J, Baty CJ, Burke NA, Watkins SC, Stolz DB, Wells A (2006). Spatial localization of m-calpain to the plasma membrane by phosphoinositide biphosphate binding during epidermal growth factor receptor-mediated activation. Mol Cell Biol 26, 5481–5496.
Shcherbina A, Bretscher A, Kenney DM, Remold-O'Donnell E (1999). Moesin, the major ERM protein of lymphocytes and platelets, differs from ezrin in its insensitivity to calpain. FEBS Lett 443, 31–36.
Shuster CB, Herman IM (1995). Indirect association of ezrin with F-actin: isoform specificity and calcium sensitivity. J Cell Biol 128, 837–848.
Srivastava J, Elliott BE, Louvard D, Arpin M (2005). Src-dependent ezrin phosphorylation in adhesion-mediated signaling. Mol Biol Cell 16, 1481–1490.

Theisen U, Straube E, Straube A (2012). Directional persistence of migrating cells requires Kif1C-mediated stabilization of trailing adhesions. Dev Cell 23, 1153–1166.
Ueyama H, Kumamoto T, Fujimoto S, Murakami T, Tsuda T (1998). Expression of three calpain isoform genes in human skeletal muscles. J Neurol Sci 155, 163–169.
Webb BA, Jia L, Eves R, Mak AS (2007). Dissecting the functional domain requirements of cortactin in invadopodia formation. Eur J Cell Biol 86, 189–206.
Webb DJ, Donais K, Whitmore LA, Thomas SM, Turner CE, Parsons JT, Horwitz AF (2004). FAK-Src signalling through paxillin, ERK and MLCK regulates adhesion disassembly. Nat Cell Biol 6, 154–161.
Weiger MC, Vedham V, Stuelten CH, Shou K, Herrera M, Sato M, Losert W, Parent CA (2013). Real-time motion analysis reveals cell directionality as an indicator of breast cancer progression. PloS One 8, e58859.
Yamaguchi H (2012). Pathological roles of invadopodia in cancer invasion and metastasis. Eur J Cell Biol 91, 902–907.
Yao X, Thibodeau A, Forte JG (1993). Ezrin-calpain I interactions in gastric parietal cells. Am J Physiol 265, C36–46.
Youn JY, Wang T, Cai H (2009). An ezrin/calpain/PI3K/AMPK/eNOSs1179 signaling cascade mediating VEGF-dependent endothelial nitric oxide production. Circ Res 104, 50–59.
Yu Y, Khan J, Khanna C, Helman L, Meltzer PS, Merlino G (2004). Expression profiling identifies the cytoskeletal organizer ezrin and the developmental homeoprotein Six-1 as key metastatic regulators. Nat Med 10, 175–181.
Zaarour RF, Chirivino D, Del Maestro L, Daviet L, Atfi A, Louvard D, Arpin M (2012). Ezrin ubiquitylation by the E3 ubiquitin ligase, WWP1, and consequent regulation of hepatocyte growth factor receptor activity. PloS One 7, e37490.
Zaidel-Bar R, Ballestrem C, Kam Z, Geiger B (2003). Early molecular events in the assembly of matrix adhesions at the leading edge of migrating cells. J Cell Sci 116, 4605–4613.
Zaidel-Bar R, Cohen M, Addadi L, Geiger B (2004). Hierarchical assembly of cell-matrix adhesion complexes. Biochem Soc Trans 32, 416–420.
Zaidel-Bar R, Milo R, Kam Z, Geiger B (2007). A paxillin tyrosine phosphorylation switch regulates the assembly and form of cell-matrix adhesions. J Cell Sci 120, 137–148.